An *Operando* Raman, IR, and TPSR Spectroscopic Investigation of the Selective Oxidation of Propylene to Acrolein over a Model Supported Vanadium Oxide Monolayer Catalyst

Chunli Zhao and Israel E. Wachs*

Operando Molecular Spectroscopy and Catalysis Laboratory, Departments of Chemistry and Chemical Engineering, 7 Asa Drive, Sinclair Laboratory, Lehigh University, Bethlehem, Pennsylvania 18015

Received: February 21, 2008; Revised Manuscript Received: May 9, 2008

The selective oxidation of propylene to acrolein was investigated over a well-defined supported V_2O_5/Nb_2O_5 catalyst, containing a surface vanadia monolayer, with combined *operando* Raman/IR/MS, temperature programmed surface reaction (TPSR) spectroscopy and isotopically labeled reactants ($^{18}O_2$ and C_3D_6). The dissociative chemisorption of propylene on the catalyst forms the surface allyl ($H_2C{=}CHCH_2$*) intermediate, the most abundant reaction intermediate. The presence of gas phase molecular O_2 is required to oxidize the surface H* to H_2O and prevent the hydrogenation of the surface allyl intermediate back to gaseous propylene (Langmuir−Hinshelwood reaction mechanism). The $^{18}O_2$ labeled studies demonstrate that only lattice ^{16}O is incorporated into the acrolein reaction product (Mars−van Krevelen reaction mechanism). This is the *first time* that a combined Langmuir−Hinshelwood−Mars−van Krevelen reaction mechanism has been found for a selective oxidation reaction. Comparative studies with allyl alcohol ($H_2C{=}CHCH_2OH$) and propylene ($H_2C{=}CHCH_3$) reveal that the oxygen insertion step does not precede the breaking of the surface allyl C−H bond. The deuterium labeled propylene studies show that the second C−H bond breaking of the surface allyl intermediate is the rate-determining step. These new observations have been incorporated in the derivation of the overall kinetics for propylene oxidation to acrolein with the model supported V_2O_5/Nb_2O_5 catalyst.

1. Introduction

The selective catalytic oxidation of propylene ($H_2C{=}CHCH_3$) to acrolein ($H_2C{=}CHCHO$) with bulk mixed metal oxide catalysts has received much attention over the years.[1–7] The bulk Bi−Mo−O mixed oxide catalysts have received most of the emphasis in the literature because of their industrial importance-for propylene oxidation and ammoxidation.[8–14] The selective oxidation of propylene over bulk Bi−Mo−O mixed oxide catalysts has been the topic of many studies involving (*i*) analyses of the product distribution,[1] (*ii*) kinetics of oxidation of D- and ^{13}C-labeled propylene,[2] and (*iii*) reaction of propylene in the presence of gaseous molecular $^{18}O_2$ [3,4] and lattice ^{18}O-labeled catalysts.[5] These studies have provided many insights into the reaction steps of C−H bond breaking and oxygen incorporation (gas phase molecular O_2 vs bulk lattice oxygen).[6–12] It was clearly demonstrated with the aid of isotopically labeled propylene that the methyl α-hydrogen abstraction is associated with the rate-determining step (rds), but two different methyl α-hydrogen abstraction steps are involved in this oxidation reaction and their respective kinetic contributions still need to be resolved. Oxygen incorporation into propylene has been shown to involve bulk lattice oxygen above 400 °C and gaseous molecular O_2 at lower reaction temperatures,[15] but the chronology of the oxygen incorporation step relative to the second C−H bond breaking step is still being debated.[10,16–21]

Although it has been shown with the aid of deuterated propylene that the selective oxidation of propylene initially proceeds by dissociative chemisorption *via* methyl α-hydrogen abstraction to form a symmetric surface allyl intermediate ($H_2C{=}CHCH_2$*), the subsequent reaction steps of the surface allyl intermediate are still not clear. Reaction studies with allyl alcohol ($H_2C{=}CHCH_2OH$), which forms the surface allyloxy ($H_2C{=}CHCH_2O$*) intermediate, have lead researchers to suggest that the insertion of oxygen precedes the second C−H bond breaking step.[10] Research studies employing allyl iodide ($H_2C{=}CHCH_2I$), however, reported that the second C−H bond breaking step of the surface allyl intermediate precedes the oxygen insertion step.[20] Theoretical computational studies, however, do not support the participation of the surface allyloxy ($H_2C{=}CHCH_2O$*) intermediate in acrolein formation.[21]

The nature of the oxygen species (bulk lattice atomic O*, surface atomic O*, surface molecular O_2*) involved in selective propylene oxidation has also been a contentious issue in the literature.[7,8,13,21–26] It has been demonstrated with the aid of gas phase molecular $^{18}O_2$ that bulk lattice oxygen is involved in the surface intermediate oxidation step at elevated reaction temperatures [7,8,13] and the role of gaseous O_2 is to reoxidize the reduced catalyst sites.[22] The reaction between the surface allyl intermediate with chemisorbed molecular O_2* to form a surface hydroperoxide intermediate ($H_2C{=}CHCH_2OO$*) that decomposes to acrolein and water has also been proposed.[23,24] Other studies have proposed that surface atomic O* rather than surface molecular O_2* is the active form of oxygen on the catalyst.[25] Clearly, more detailed fundamental studies are required to fully understand the nature of the oxygen species present and its insertion step into the surface C_3 hydrocarbon intermediate during selective oxidation of propylene.

A major drawback of the extensively investigated bulk mixed metal oxide catalysts is that their BET surface areas are very low (∼0.1−5 m^2/g) since this limits the amount of accessible surface information (nature of catalytic active site, surface oxygen species, surface reaction intermediates, etc.). In contrast, supported metal oxide catalysts usually contain high surface areas (∼30−300 m^2/g) and the catalytic active sites are typically 100% molecularly dispersed on the high surface area support.

* To whom correspondence should be addressed. Phone: (610)-758-4274. Fax: (610)-758-6555. E-mail: iew0@lehigh.edu.

10.1021/jp801562g CCC: $40.75
Published on Web 07/03/2008

Consequently, supported metal oxide catalysts represent model catalytic systems for obtaining fundamental insights about the nature of the catalytic active sites and the surface reaction intermediates. Only a limited number of propylene oxidation studies with supported metal oxide catalysts have been undertaken to date (supported MoO_3/SiO_2, V_2O_5/SiO_2 and V_2O_5/TiO_2 catalysts) and, unfortunately, these studies primarily yielded nonacrolein products (propylene oxide, acetone and combustion) under the chosen experimental conditions.[26–31]

The selective oxidation of propylene to acrolein over model supported V_2O_5/Nb_2O_5 catalysts was recently reported by the current authors with the aid of in situ Raman, in situ IR and C_3H_6-temperature programmed surface reaction (TPSR) spectroscopy studies.[30] The most abundant surface reaction intermediate (MARI) during propylene oxidation was found to be surface allyl (H_2CCHCH_2*). The catalytic active site was found to be bridging V−O−support bond and two surface VO_x sites participate in the selective oxidation of propylene to acrolein (a 4 electron redox reaction). In addition, the reaction kinetics was found to vary with first-order in propylene partial pressure and half-order in molecular O_2 partial pressure. With the recent introduction of the *operando* spectroscopic approach to catalysis research that involves simultaneous catalyst spectroscopic characterization and online reaction product analysis to develop molecular structure−activity/selectivity relationships, there is currently a strong desire to simultaneously obtain real-time spectroscopic and kinetic details about catalytic systems under relevant reaction conditions to establish molecular/electronic structure−activity/selectivity relationships.[32,33]

The objectives of the current study are to determine for the selective oxidation of propylene to acrolein over well-defined supported V_2O_5/Nb_2O_5 catalysts (*i*) the catalytic roles of the different types of oxygen species (surface O* and O_2* from gas phase molecular O_2 and bulk O^{2-}* from the catalyst bulk lattice, (*ii*) the rds, (*iii*) the surface reaction mechanism, (*iv*) the chronology of the elementary steps, and (*v*) the reaction kinetics.

2. Experimental Section

2.1. Catalyst Preparation and Characterization. The model supported V_2O_5/Nb_2O_5 catalyst was prepared by the incipient wetness impregnation of an isopropoxide/isopropanol solution into an Nb_2O_5 support (67 m^2/g) in a glovebox under a N_2 environment, dried at room temperature overnight, initially calcined in N_2 at 300 °C for 1 h and finally calcined in air at 450 °C for 2 h. Additional details of the preparation method and the dehydrated Raman spectra of the resulting supported V_2O_5/Nb_2O_5 catalyst were previously reported.[30] The in situ Raman spectra demonstrated that crystalline V_2O_5 nanoparticles are absent in this catalyst and only a monolayer of surface VO_x species is present in the supported V_2O_5/Nb_2O_5 catalyst containing 7 wt % V_2O_5 (8.4 V/nm^2).

2.2. Raman and FT-IR Spectroscopy with Online Mass Spectrometry. The Raman and FT-IR spectra were collected under different reaction conditions with a Horiba-Jobin Yvon LabRam-IR HR system equipped with a sensitive LN_2 CCD detector (JY-CCD3000), a notch filter (532 nm) and single stage monochromator with 900 grooves/mm grating. The laser power was kept below 0.5 mW to minimize any laser induced sample changes and the spectrometer resolution was ∼1−2 cm^{-1}. The Raman spectra were collected with visible laser excitation at 532 nm (Coherent 315, YAG doubled diode pumped laser, 20 mW) in the 100−1200 cm^{-1} region with 10 s/scan, and 10 scans per spectrum for SS mode and 5 scans per spectrum for TP mode.

The IR vibrational measurements were performed with a Fourier transform infrared spectrometer (IlluminatIR II, Smith Detection) equipped with mercury telluride (HgTe) and cadmium telluride (CdTe) photoconductive detectors (MCT) and cooled using liquid nitrogen. The reflectance FT-IR spectra were collected in the total reflection mode employing 0.3 s/scan with a resolution of ∼4 cm^{-1} (1000 scans for the SS mode and 200 scans for TP mode). The current reactor system employs a modified environmental reactor cell (Harrick, HVC-DR2) for simultaneously obtaining molecular level spectroscopic and reaction kinetic data. Typically, ∼20−30 mg of the supported vanadia catalyst was placed into the reaction cell as loose powder. The composition of the reactant gaseous feed was controlled with mass flow controllers (Brooks 5850E) and the total gas flow rate was maintained at 30 mL/min. The gaseous outlet from the flow-through fixed-bed reactor was connected to an online mass spectrometer (Varian, 1200L quadrupole). The online MS spectra were collected every 0.5s. The *m/e* values used to detect the reactants and products were *m/e* = 41 for C_3H_6, *m/e* = 56 for CH_2=CHCHO (acrolein), *m/e* = 58 for CH_3COCH_3 (acetone), *m/e* = 55 for CH_2=CHCOOH (acrylic acid), *m/e* = 28 for CO and *m/e* = 44 for CO_2. The Raman and IR spectra were collected under reaction conditions with the simultaneous MS analysis of the reaction product stream to constitute the *operando* spectroscopy experimental mode.

2.3. *Operando* Experimental Protocols. The *operando* Raman/FT-IR/MS spectroscopy measurements were obtained under steady-state (SS) as well as temperature programmed (TP) modes.

In the *operando* SS mode, the catalyst was also placed inside the Harrick cell as loose powder, heated to 450 °C for 30 min under flowing 5% O_2/He to dehydrate the catalyst and remove any combustible impurities that may be present and subsequently cooled down to the reaction temperature of 300 °C in flowing 5% O_2/He. Propylene was subsequently introduced into the flowing gas stream to form a reaction mixture of C_3H_6/O_2 = 1:4 (2.96% C_3H_6/He, Scott Specialty Gases; 99.996% purity O_2 balanced in ultrahigh purity He). In the *operando* SS mode, transient isotopic $^{18}O_2$ (5% $^{18}O_2$/He with 97% $^{18}O_2$ purity, Matheson Specialty Gases) experiments were also performed to determine the roles of gas phase molecular O_2 and surface lattice oxygen in the propylene selective oxidation reaction. After 20 min, the isotopic switch from $^{16}O_2$ to $^{18}O_2$ was performed and was subsequently also reversed after 20 min. Parallel *operando* Raman/FT-IR/MS SS experiments were also performed to examine isotopic kinetic effect for the oxidation of the propylene isotopes C_3H_6 and C_3D_6 as a function of reaction temperature (50, 70, 100, 150, 200, 250, and 300 °C).

In the *operando* TP mode, the catalyst sample was also initially calcined at 450 °C for 30 min in flowing 5% O_2/He. The dehydrated Raman spectrum was collected after cooling the sample to 50 °C in the flowing O_2/He. Propylene was subsequently adsorbed onto the catalyst by flowing 2.96% C_3H_6/He at 50 °C for 30 min in either flowing 5% O_2/He flow or pure He to examine the influence of gaseous O_2. The catalyst was subsequently flushed with either He or O_2/He to remove any residual physically adsorbed C_3H_6 prior to initiating the temperature programmed experiment. The catalyst temperature was then increased at a rate of 10 °C/min to 400 °C flowing either He or O_2/He. The Raman spectra were collected every 50 °C, the IR spectra were collected every 25 °C, and the MS analysis was performed every 0.5 s.

Isotopically labeled 3.3% C_3D_6/He (Isotec, Ultra High Purity) was also employed in the *operando* TP mode experiments with

the same experimental conditions described above for C_3H_6. The MS *m/e* values used to detect the reactants and products were *m/e* = 47 for C_3D_6 (propylene-D), *m/e* = 60 for CD_2=CDCDO (acrolein-D), *m/e* = 64 for CD_3COCD_3 (acetone), *m/e* = 59 for CD_2=CDCOOD (acrylic acid), *m/e* = 28 for CO, and *m/e* = 44 for CO_2.

Operando Raman/FT-IR/MS spectroscopy SS and TP measurements with allyl alcohol, H_2C=$CHCH_2OH$ (1980 ppm CH_2=$CHCH_2OH$/He, 99% purity, GTS), were also performed in order to examine the surface chemistry of the surface allyloxy (H_2C=$CHCH_2O$*) intermediate since alcohols are known to dissociative adsorb by breaking their O−H bond.[34] In the SS mode, the dehydrated catalysts were exposed to a CH_2=$CHCH_2OH/O_2$ = 1:4 and balance ultra-high purity He gas mixture. The SS reaction temperature was maintained at 50, 100, 150, 200, 250 and 300 °C until a stable MS signal was obtained (~30 min). The *operando* SS Raman and IR spectra were also collected at each temperature and the MS analysis was recorded every 0.5 s. In the *operando* TP mode, after the catalyst pretreatment, the catalyst was exposed at 70 °C for 30 min to a CH_2=$CHCH_2OH$/He gas mixture (1980 ppm CH_2=$CHCH_2OH$/He, 99% purity, GTS) to dissociative chemisorbed allyl alcohol as surface allyloxy (H_2C=$CHCH_2O$*) on the catalyst and, subsequently temperature programmed at 10 °C/min until 400 °C in flowing He. The *operando* TP Raman and IR spectra were collected every 50 and 25 °C, respectively, and the MS analysis was performed every 0.5 s.

2.4. C_3H_6−Temperature Programmed Surface Reaction (TPSR) Spectroscopy. Additional TPSR experiments were conducted to better determine the roles of gas phase molecular O_2 and lattice oxygen from the catalyst during propylene oxidation to acrolein. These C_3H_6-TPSR experiments were performed with a conventional Altamira Instruments temperature programmable system (AMI-200) equipped with an online quadrupole MS (Dycor Dymaxion, DME200MS). Typically, ~200 mg of the supported V_2O_5/Nb_2O_5 catalyst was loaded into a U-shaped quartz tube and initially calcined at 450 °C in flowing air (Air Products, Ultra Zero grade Air, 30 mL/min) for 60 min to remove adsorbed moisture and any combustible impurities that may be present. The pretreated catalyst was cooled down in flowing air to 110 °C and the flowing gas stream was subsequently switched to the ultra high purity He upon further cooling to 70 °C for 30 min. Subsequently, propylene was adsorbed on the catalyst surface by flowing 2.96% C_3H_6/He for 30 min. The different experimental TPSR protocols employed are described in Table 1. Step 1 refers to the gases (He, $^{16}O_2$ or $^{18}O_2$) present during the propylene adsorption process, and step 2 refers to the gases (He, $^{16}O_2$ or $^{18}O_2$) present during the TPSR experiment.

TABLE 1: C_3H_6−TP/TPSR Experimental Protocol and Acrolein Formation

experiment	step 1	step 2	acrolein formation
A	He	He	no
B	$^{16}O_2$	$^{16}O_2$	acrolein-^{16}O
C	$^{16}O_2$	He	acrolein-^{16}O
D	He	O_2	no
E	$^{16}O_2$	$^{18}O_2$	acrolein-^{16}O
F	$^{18}O_2$	$^{16}O_2$	acrolein-^{16}O

3. Results

3.1. *Operando* Raman and FT-IR Spectroscopy with Online Mass Spectrometry. ***3.1.1. Operando Spectroscopy in C_3H_6-TP Mode.*** *Operando* C_3H_6-TP spectroscopy experiments were undertaken with the model monolayer supported V_2O_5/Nb_2O_5 (8.4 V/nm^2) catalyst in order to investigate the influence of gaseous molecular O_2 upon propylene oxidation to acrolein. According to Table 1 experiment A and B, the C_3H_6-TP spectra in the absence as well as presence of flowing gaseous O_2 are presented in panels a and b of Figure 1, respectively. The O_2-free C_3H_6-TP spectra in Figure 1a reveal that the main reaction product from propylene oxidation by the catalyst lattice oxygen is CO_2 (Tp values of 152, 249 and 361 °C). Small amounts of acetone are also detected at Tp values of 152 and 225 °C. Acrolein and acrylic acid, however, are not formed in the absence of gaseous molecular O_2. Reaction-limited C_3H_6 also desorbs with a Tp ≈ 146 °C, which occurs at significantly higher temperatures than desorption of physisorbed propylene.[35,36] In the presence of gaseous molecular O_2, the C_3H_6-TP spectra in Figure 1b exhibit acrolein as the main reaction product (Tp values of 198 and 307 °C, with most of the acrolein appearing at the lower temperature). The production of CO_2, acetone and C_3H_6 are greatly diminished with the C_3H_6 amount decreasing by ~50%. A more detailed comparison of acrolein production in the presence and absence of gas phase molecular O_2 during the C_3H_6-TP experiments is presented in Figure 1c. Only a trace of acrolein is formed when propylene is both chemisorbed and reacted with the catalyst in flowing He (Tp ≈ 198 °C) compared to the significant production of acrolein when flowing O_2 is present during both propylene chemisorption and the C_3H_6-TP experiment (Tp ≈ 198 and 307 °C). Thus, the presence of gas phase molecular O_2 is critical for the selective oxidation of propylene to acrolein over the supported V_2O_5/Nb_2O_5 monolayer catalyst.[30]

The corresponding *operando* IR spectra were also obtained during the propylene oxidation C_3H_6-TP experiment. The IR spectra for the O_2-free experiment are presented in Figure 2a and that with O_2 present in Figure 2b. In the presence as well as absence of gaseous O_2, the C−*C*−*H* stretching band of the surface allyl intermediate (CH_2=$CHCH_2$*) is observed at 2987 cm^{-1} and is similar to the C−H stretch previously found at 2960 cm^{-1} for the surface $CH_3CH_2CH_2CH_2$* intermediate.[37] The surface allyl IR peak is no longer present on the catalyst surface at ~170 °C and higher temperatures, which suggests that it has been converted to a reaction product. The IR intensity of the surface allyl intermediate peak at 2987 cm^{-1} is stronger in the presence of molecular O_2 (compare panels a and b of Figure 2), which indicates that the presence of molecular O_2 enhances formation of surface allyl species on the catalyst.

The temperature dependence of the surface allyl intermediate IR signal and the acrolein gas phase formation signal in the MS are shown in Figure 3. Note that the surface allyl intermediate signal dramatically decreases as the gaseous acrolein formation increases and further emphasizes the relationship between these two molecules.

The complementary *operando* Raman spectra in panels a and b of Figure 4 show the effect of absence and presence of gaseous O_2 on the terminal *V*=O band at 1036 cm^{-1}, respectively.[30] The Raman spectra exhibit a somewhat stronger *V*=O band at 1036 cm^{-1} in the presence of gaseous O_2. A comparison of the Raman spectra appears in Figure 4c in which the Raman spectra at a reaction temperature of 300 °C are normalized with respect to the Nb_2O_5 support band at ~935 cm^{-1}.[30] The stronger *V*=O Raman band in the presence of gas phase molecular O_2 reflects

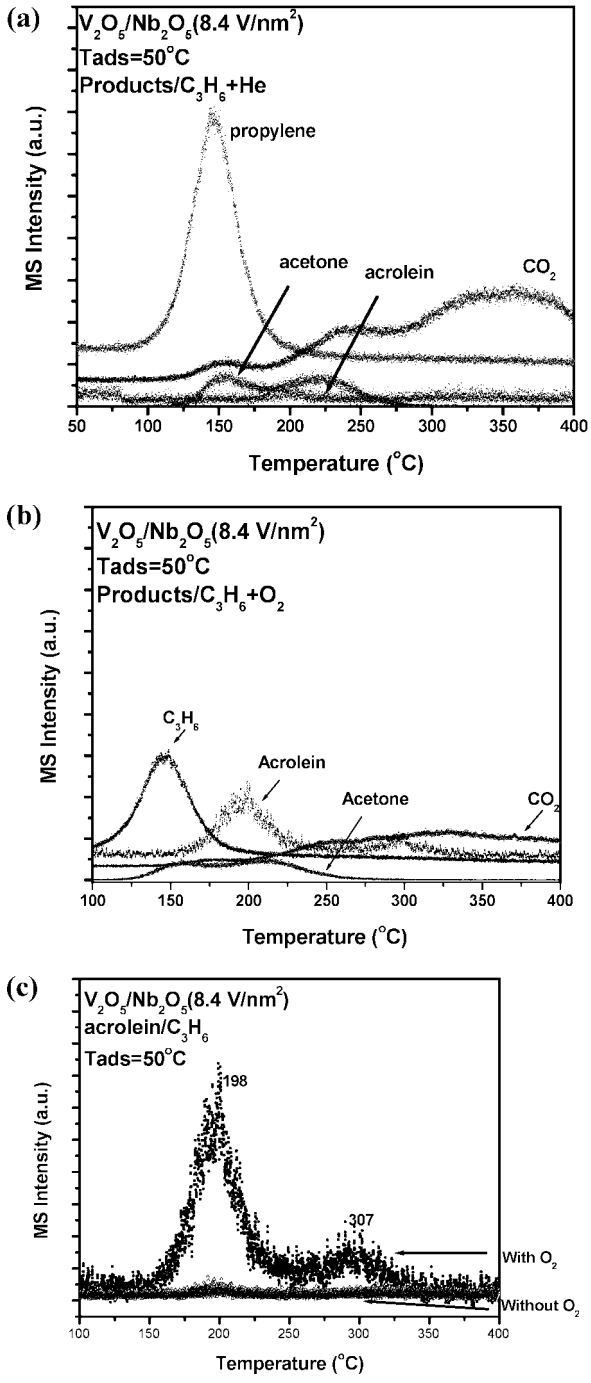

Figure 1. (a) *Operando* MS spectra in C_3H_6-TP mode with flowing helium for both C_3H_6 chemisorption and surface reaction steps. (b) *Operando* MS spectra in C_3H_6-TP mode with flowing O_2/He for both C_3H_6 chemisorption and surface reaction steps. (c) Comparison of acrolein formation during *operando* TP mode with/without gaseous molecular O_2 present during C_3H_6 chemisorption and surface reaction.

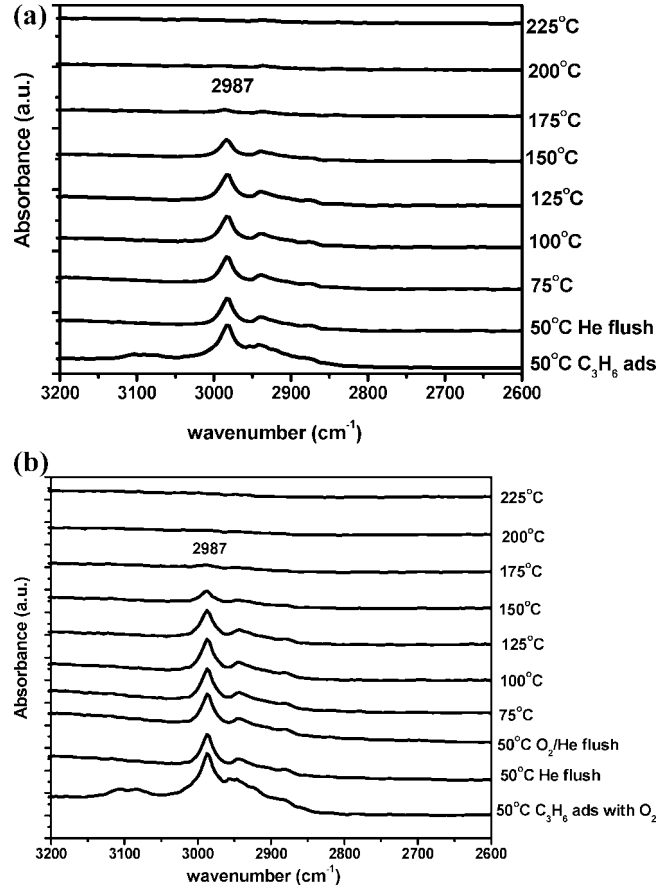

Figure 2. (a) *Operando* IR spectra in C_3H_6-TP mode with flowing helium for both C_3H_6 chemisorption and surface reaction steps. (b) *Operando* IR spectra in C_3H_6-TP mode with flowing O_2/He for both C_3H_6 chemisorption and surface reaction steps.

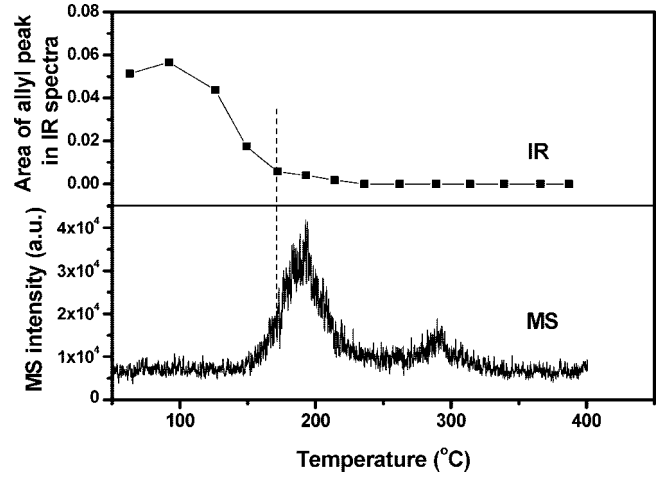

Figure 3. Temperature dependence of surface allyl intermediate IR signal and gas phase acrolein formation from the MS signal.

the partial reduction of the surface VO_4 species in the reducing C_3H_6/He environment.[30,39] The extent of reduction of the *V*═O Raman band, however, is rather minor suggesting that bulk lattice oxygen is supplying the oxygen atoms to the surface VOx species in the absence of gas phase molecular O_2. At elevated temperatures, for both experimental conditions, the terminal *V*═O Raman band at 1036 cm^{-1} becomes stronger above 200 °C after the surface allyl intermediate has reacted and the products desorbed from the catalyst surface. Such Raman trends are typical since hydrogen bonding at the *V*═O sites from the surface intermediates are responsible for band broadening.[32,33] Furthermore, Raman vibrations in the 800−1200 cm^{-1} region for surface molecular O_2* species (surface peroxides O_2^{2-} and super oxides O_2^-) are not present in the 50−400 °C temperature range (see Figure 4b).[38]

3.1.2. Operando Spectroscopy in SS Mode with Isotopic Switching of Molecular O_2. Transient isotopic $^{16}O_2-^{18}O_2$ switching experiments during SS propylene oxidation were further undertaken to determine the role of gaseous molecular O_2 during the selective oxidation of propylene to acrolein. The

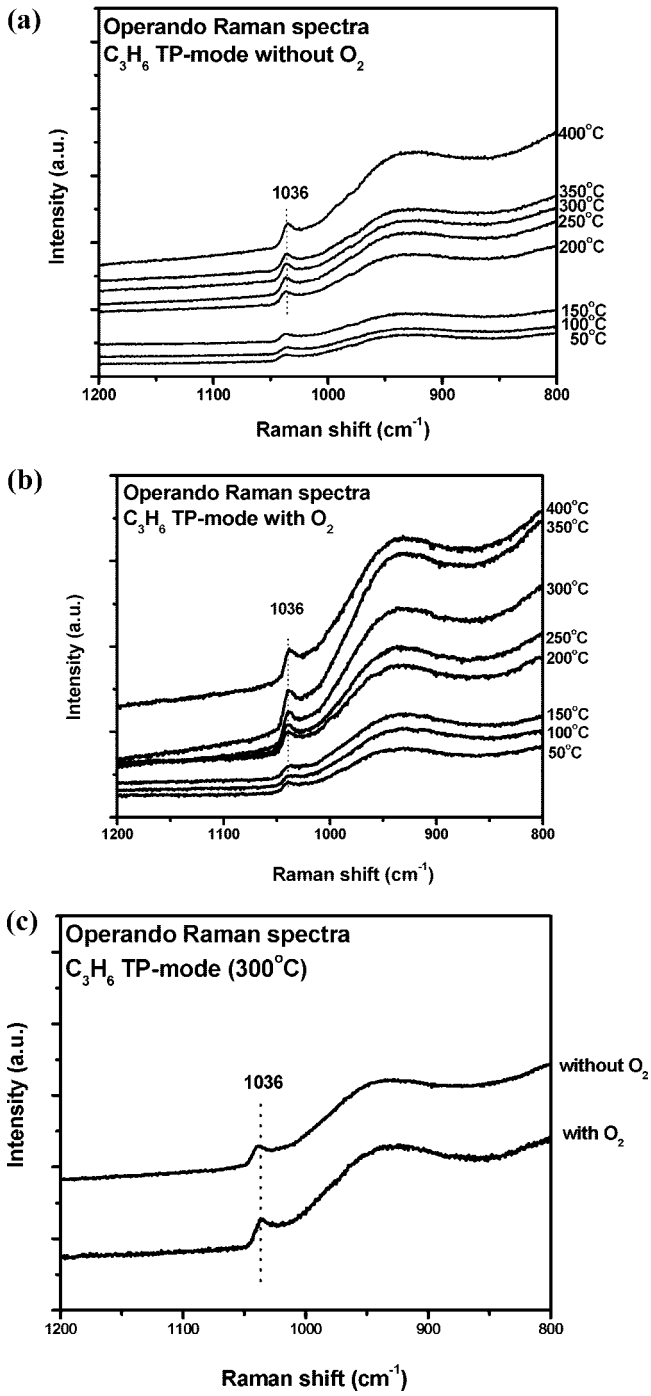

Figure 4. (a) *Operando* Raman spectra in C_3H_6-TP mode without O_2 from C_3H_6 chemisorption and reaction. (b) *Operando* Raman spectra in C_3H_6-TP mode with O_2 from C_3H_6 chemisorption and surface reaction. (c) Comparison of Raman spectra with and without gas phase molecular O_2 at 300 °C (normalized with respect to the Nb_2O_5 support band).

resulting time-resolved formation of the oxygen-containing reaction products, $H_2C{=}CHCHO$ and CO_2, and their isotopic oxygen distributions were monitored with the online MS and shown in Figure 5. A 1:4 $C_3H_6/^{16}O_2$ ratio was introduced into the catalytic reactor system and the steady-state MS signal was reached after ~20 min. The isotopic switch from $^{16}O_2$ to $^{18}O_2$ did not initially yield $H_2C{=}CHCH^{18}O$ and $C^{18}O_2$ reaction products and only the ^{16}O-containing reaction products continued to form. Approximately 25 min after the $^{16}O_2{-}^{18}O_2$ isotopic switch, small amounts of $H_2C{=}CHCH^{18}O$ and $C^{18}O_2$ began to

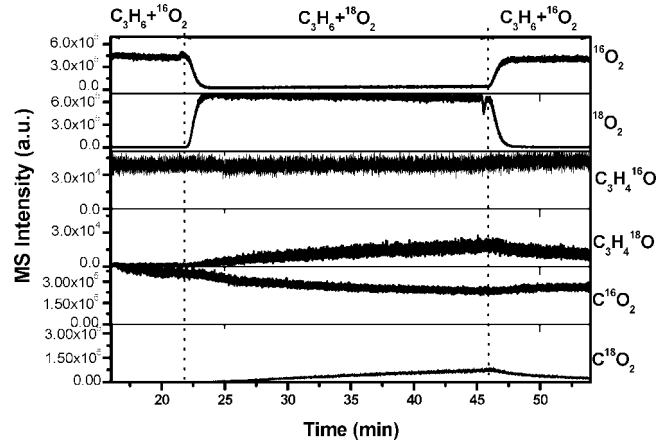

Figure 5. *Operando* MS signals for O_2, $H_2C{=}CHCHO$, and CO_2, with both $^{16}O_2$ and $^{18}O_2$, during the transient isotopic $^{18}O_2{-}^{16}O_2$ switching experiment for SS propylene oxidation at 300 °C.

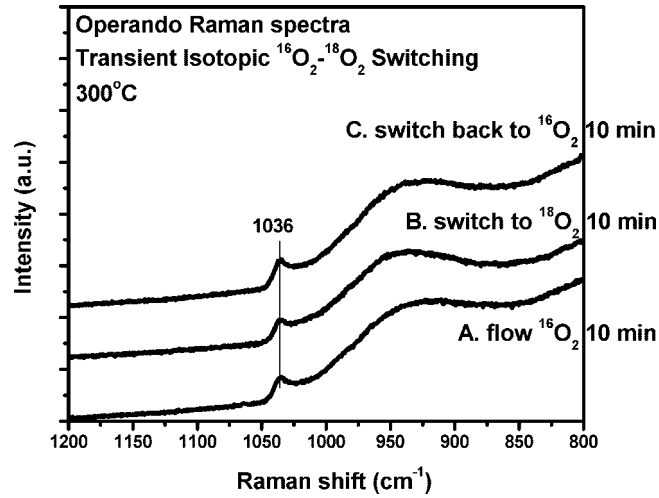

Figure 6. *Operando* Raman spectra during the transient isotopic $^{18}O_2{-}^{16}O_2$ switching experiment for SS propylene oxidation at 300 °C.

appear and their concentrations slowly increased with time. Upon switching back from $^{18}O_2$ to $^{16}O_2$, the isotopically labeled $H_2C{=}CHCH^{18}O$ and $C^{18}O_2$ reaction products sluggishly decreased with time over a ~25 min period. The ^{18}O containing products only completely diminished when the propylene flow was terminated indicating that some ^{18}O was incorporated in the catalyst lattice. These isotopic $^{16}O_2{-}^{18}O_2$ switching SS experiments reveal that the oxygen incorporated into both acrolein and CO_2 reaction products originates from the lattice oxygen of the supported V_2O_5/Nb_2O_5 catalyst rather than directly from the gaseous molecular O_2.

The corresponding *operando* Raman spectra at 300 °C are presented in Figure 6. The Raman spectra show that the $V{=}^{16}O$ band at 1036 cm^{-1} does not change position during the isotopic switch and that a new $V{=}^{18}O$ band at 990 cm^{-1} is not present.[39] As before, Raman bands from surface molecular $^{18}O_2$* species in the 800−1200 cm^{-1} region are not present.[38] The corresponding FT-IR spectra during the SS isotopic switching experiments were also collected, but are not shown since the low concentration of the surface allyl intermediates at 300 °C was below the FT-IR detection limit.

3.2. C_3H_6-TPSR Spectroscopy. ***3.2.1. Influence of Gas Phase Molecular O_2 and Lattice Oxygen.*** Additional C_3H_6-TPSR spectroscopy experiments were undertaken to further investigate the influence of gas phase molecular O_2 upon

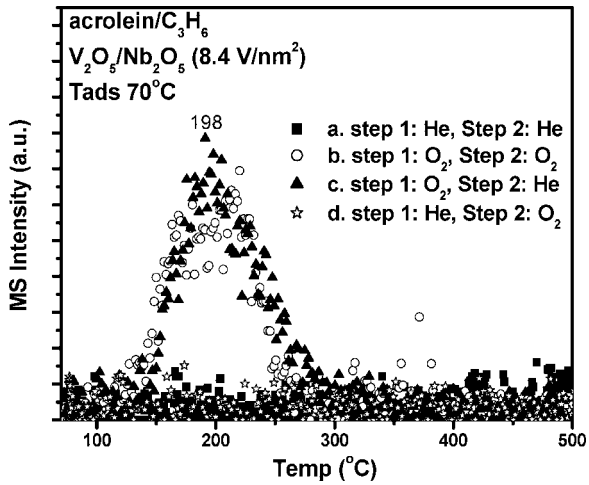

Figure 7. Influence of gaseous molecular O_2 upon acrolein formation from propylene oxidation during C_3H_6-TPSR spectroscopy.

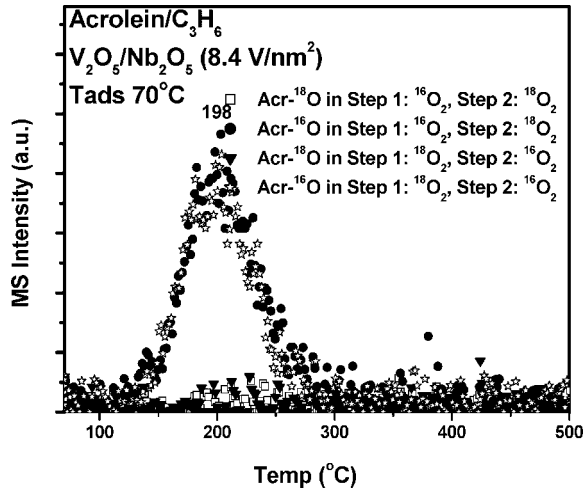

Figure 8. Influence of gaseous molecular $^{18}O_2$ upon C_3H_6-TPSR spectroscopy. Experimental conditions: (e) $^{16}O_2$ in step 1 and $^{18}O_2$ in step 2; (f) $^{18}O_2$ in step 1 and $^{16}O_2$ in step 2.

propylene adsorption (step 1) and oxygen insertion (step 2). The experimental protocol and acrolein formation are presented and summarized in Table 1, respectively. The C_3H_6-TPSR spectral results from experiments a−d in Table 1 are presented in Figure 7 and demonstrate that acrolein is only formed when gaseous molecular O_2 is present during the propylene chemisorption step. The corresponding C_3H_6-TPSR experiments e and f in Table 1 with molecular $^{16}O_2$ and $^{18}O_2$ are shown in Figure 8 and reveal that ^{18}O-containing acrolein is not produced in the presence of molecular $^{18}O_2$, which is consistent with the isotopic switching $^{16}O_2-^{18}O_2$ experiments presented above. This experimental observation further indicates the exclusive incorporation of bulk lattice ^{16}O from the supported V_2O_5/Nb_2O_5 catalyst in the acrolein reaction product.

3.2.2. Influence of Isotopic C_3D_6. The kinetic isotope effect for C_3H_6- and C_3D_6-TP experiments was also investigated. In these experiments, C_3H_6 and C_3D_6 were individually adsorbed in the presence of O_2 on the supported V_2O_5/Nb_2O_5 catalyst surface and the acrolein (H_2C═CHCHO) and deuterated acrolein (D_2C═CDCDO) reaction products were monitored with the online MS (Figure 9). Such experiments provide molecular insights into the C−H bond breaking steps since C−D bonds are stronger than C−H bonds.[11,12] The Tp value for breaking the surface allyl C−D bond is 19 °C higher with C_3D_6 than the surface allyl C−H bond with C_3H_6. Such a significant shift in

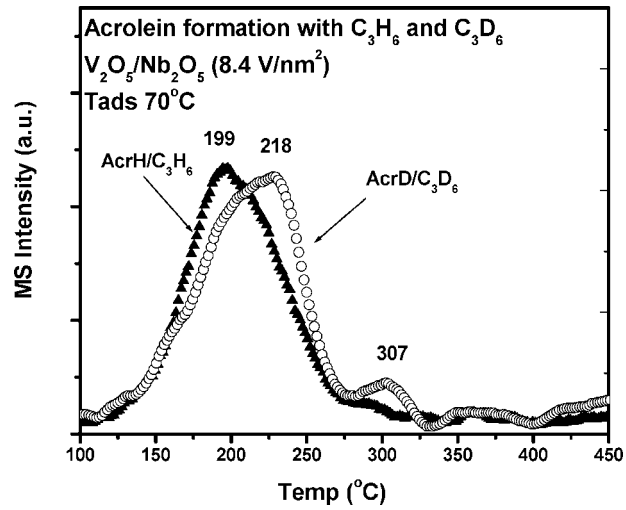

Figure 9. Comparison of H_2C═CHCHO and D_2C═CDCDO formation from C_3H_6-TPSR and C_3D_6-TPSR spectroscopy, respectively. Experiments conducted with O_2 present during propylene chemisorption.

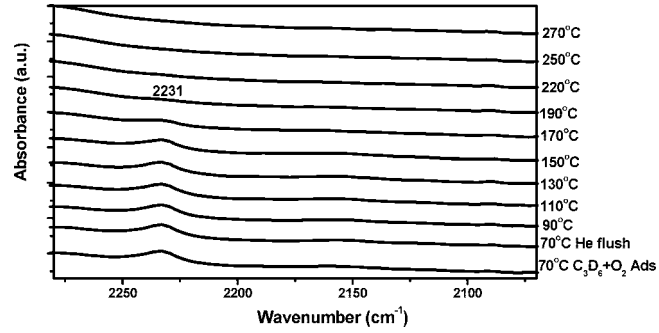

Figure 10. *Operando* IR spectra during C_3D_6-TP spectroscopy.

Tp reflects the strong influence of breaking the surface allyl α-C−H bond on the surface reaction kinetics, especially the rds. The corresponding activation energy (E_{act}) values obtained by use of the Redhead equation for acrolein formation from C_3H_6 and C_3D_6 are 32.0 and 33.6 kcal/mol translate to a kinetic isotope effect of $k_{C3H6}/k_{C3D6} \approx 3.2$ at 300 °C.

Corresponding *operando* IR spectroscopy measurements in Figures 2b and 10 confirm the C_3H_6-TPSR spectroscopy findings since the surface C_3H_5* intermediate is almost completely reacted away at 170 °C while the surface C_3D_5* intermediate requires a temperature of ∼190 °C to be completely reacted away. Correction of the intensity of the IR spectra in Figures 2b and 10 for the different flow rates of $C_3D_6/C_3H_6 = 1:2$ and extinction coefficients of the surface C_3H_5*/C_3D_5* [40,41] results in an IR surface C_3H_5*/C_3D_5* ratio of ∼1 between 70 and 150 °C. The comparable amounts of surface C_3H_5* and C_3D_5* indicates that breaking of the initial methyl α-C−H bond during propylene chemisorption is not related to the rds for propylene oxidation over the supported V_2O_5/Nb_2O_5 catalysts.

The SS kinetic isotope effect (KIE) for both C_3H_6/C_3D_6 consumption and C_3H_4O/C_3D_4O production at 300 °C gives a KIE value of 2.9−3.1. The SS KIE confirms the role of C−H bond breaking in the rds during propylene oxidation to acrolein.

3.3. *Operando* H_2C═$CHCH_2OH$ in SS and TP Modes. The CH_2═$CHCH_2OH$-TP mass spectra in flowing helium are presented in Figure 11 and exhibit acrolein as the main reaction product with a Tp value of 163 °C. In addition, desorption of some allyl alcohol takes place with a Tp of 157 °C and a trace amount of acetone is also formed. The distribution of reaction products reflects the redox character of the monolayer supported V_2O_5/Nb_2O_5 catalyst since

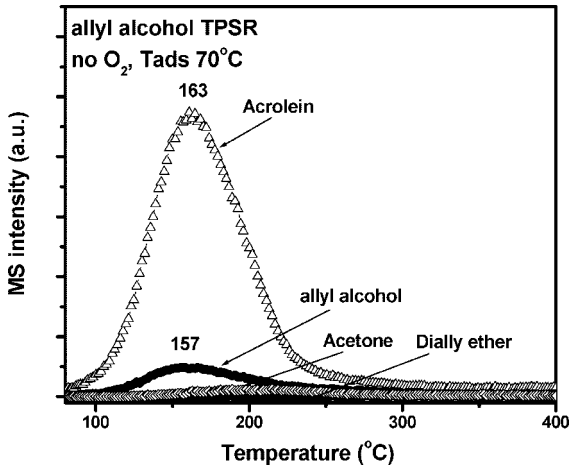

Figure 11. *Operando* MS spectra in TP mode from $CH_2{=}CHCH_2OH$ chemisorption and surface reaction.

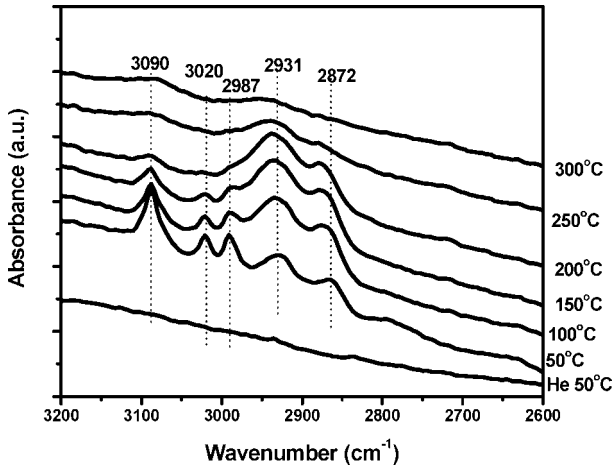

Figure 12. *Operando* IR spectra during allyl alcohol oxidation in SS-mode.

ally alcohol should yield acrolein from surface redox sites and diallyl ether from surface acidic sites.

The complementary *operando* $CH_2{=}CHCH_2OH$-SS oxidation reaction was also investigated with a $C_3/O_2 = 1{:}4$ ratio from 50 to 300 °C. Conversion of allyl alcohol and acrolein formation was not observed below 100 °C. In the intermediate temperature range of 100−200 °C, conversion of allyl alcohol and formation of acrolein, with some minor CO_2, was found to take place. Above 200 °C, CO_2 became the dominant reaction product and is the only reaction product above 300 °C.

The corresponding *operando* IR spectra in SS-mode are shown in Figure 12 for the 3200−2600 cm^{-1} range. Below 200 °C, the $C{=}C{-}H$ stretching modes at 3090, 3020 and 2987 cm^{-1} arise from the chemisorbed allyloxy ($H_2C{=}CHCH_2O$*) intermediate.[37,42] The additional IR bands at 2931 and 2872 cm^{-1} are assigned to $-C{-}H$ asymmetric and symmetric stretching modes of surface carboxylates.[43,44] These carboxylates species initially grow with temperature and are not present above 250 °C at which the complete combustion of allyl alcohol takes place. Comparison of the IR spectra during allyl alcohol oxidation (Figure 12) with the IR spectra during propylene oxidation (Figure 2) clearly reveals that surface allyloxy ($H_2C{=}CHCH_2O$*) is not a reaction intermediate during propylene oxidation to acrolein.

4. Discussion

The *operando* C_3H_6-TP mode spectra demonstrate that gas phase molecular O_2 is required for the selective oxidation of propylene to acrolein as shown in Figure 1. The corresponding *operando* IR spectra depicted in Figure 2 further confirm that the dissociative chemisorption of propylene to surface allyl on the catalyst is enhanced by the presence of gaseous molecular O_2. These experimental findings that both gas phase C_3H_6 and molecular O_2 are required for acrolein formation are consistent with a Langmuir−Hinshelwood (L-H) reaction mechanism.

The *operando* spectroscopy in SS mode with the isotopic $^{16}O_2{-}^{18}O_2$ switching experiments, however, suggest that propylene oxidation to acrolein follows a Mars−van Krevelen (MVK) reaction mechanism (see Figure 5). The sluggish response in the appearance of acrolein-O^{18} during gas phase $^{16}O_2{-}^{18}O_2$ switching indicates that lattice oxygen from the catalysts plays a key role in the selective oxidation of propylene to acrolein. The corresponding *operando* Raman spectra reveal that the terminal $V{=}^{16}O$ bond of the catalytic active surface vanadia site does not undergo any significant isotopic shift to $V{=}^{18}O$ when gas phase $^{16}O_2$ switched to $^{18}O_2$ (see Figure 6). These experimental findings are consistent with a significant participation of active lattice ^{16}O* that is stored in the bulk of the supported V_2O_5/Nb_2O_5 catalyst.

Additional insights into the roles of gas phase molecular O_2 and catalyst lattice oxygen during propylene oxidation to acrolein are provided from the C_3H_6-TPSR spectroscopy experiments with the aid of isotopic $^{16}O{-}^{18}O$ labeling. The C_3H_6-TPSR measurements allowed for the independent investigation of the influence of gas phase molecular O_2 and lattice O* from the catalyst for acrolein formation. Acrolein is only produced when gas phase molecular O_2 is present during the propylene dissociative chemisoprtion step (see Table 1). This suggests that surface oxygen supplied by gaseous molecular O_2 is required to oxidize the surface H* to H_2O in order to prevent the reversible hydrogenation of the surface C_3H_5* intermediate back to propylene, which is consistent with a Langmuir−Hinshelwood reaction mechanism. The presence of gaseous molecular O_2 does not affect the surface allyl oxidation step since the same surface kinetics (same Tp value) occur in the presence and absence of gaseous molecular O_2 during the TPSR reaction step (see Figure 8). Furthermore, only acrolein-^{16}O is formed in the presence of gaseous molecular $^{18}O_2$ during propylene adsorption and surface allyl oxidation steps. This observation shows that the oxygen inserted into the surface allyl intermediate originates from the catalyst lattice oxygen via a Mars−van Krevelen mechanism (see Table 1 and Figure 8).

The functions of gaseous molecular O_2 during propylene oxidation to acrolein are (*i*) to remove the surface H* species by oxidation to H_2O, and (*ii*) to replenish the reduced lattice oxygen sites. The latter function is demonstrated by the isotopic oxygen switching experiments that exhibit the sluggish formation of $H_2C{=}CH^{18}O$ after the $^{16}O_2$-$^{18}O_2$ switch as well as after the reverse $^{18}O_2{-}^{16}O_2$ switch of the reactant stream (see Figure 5). The continued formation of some $H_2C{=}CH^{18}O$ after $^{18}O_2$ is removed from the reactant stream clearly shows the catalyst lattice reoxidation character. Furthermore, the *operando* Raman spectra also show minor reduction of the surface vanadia species during propylene oxidation (see Figures 4 and 6). Raman spectroscopy, however, does not reveal the presence of surface molecular O_2* species, either surface peroxides or superoxides, during propylene chemisorption and oxidation in the presence of gas phase O_2 (see Figures 4 and 6). Surface molecular O_2* species tend to give rise to strong Raman bands because of the high electron density in the O−O bond.[38] Consequently, the surface oxygen species most likely responsible for oxidation of H* to water is surface O*. A surface

O* species, however, would give rise to weak Raman bands at ~800−900 cm^{-1} that is difficult to detect against the strong background of the niobia support in this region.

The above findings reveal that the selective oxidation of propylene to acrolein proceeds via a Langmuir−Hinshelwood mechanism during the dissociative chemisorption step (both C_3H_6 and O_2 must be present) and a Mars−van Krevelen reaction mechanism during the surface allyl oxygen insertion step (catalyst lattice oxygen provides the oxygen). This is *the first time* that a combined Langmuir−Hinshelwood−Mars−van Krevelen (L-H-M-V-K) reaction mechanism has been found to be operative for a selective oxidation reaction.

Additional insights into the rds of propylene oxidation to acrolein over the model supported V_2O_5/Nb_2O_5 catalyst are provided from the isotopically labeled C_3H_6 and C_3D_6 experiments. A KIE of 2.9−3.1 is obtained when C_3H_6 is substituted by C_3D_6 during propylene oxidation at 300 °C. Furthermore, the C_3-TPSR spectra show that the Tp for acrolein formation occurs at ~19 °C higher for C_3D_6 than C_3H_6 (see Figure 9). This significant kinetic isotope shift in Tp with the deuterated propylene, which corresponds to a KIE of 3.2 at 300 °C, and the SS KIE of 2.9−3.2 demonstrate the important kinetic contribution of breaking the surface allyl α−C-H bond in acrolein formation. This is also reflected in the *operando* IR spectra that show that surface C_3H_5* disappears at ~170 °C and surface C_3D_5* disappears at ~190 °C (compare Figures 2b and 10) as well as in the corresponding appearance of reaction limited C_3H_6 and C_3D_6 production. Thus, α-C−H bond breaking is involved in the rds for propylene oxidation to acrolein.

Although the α-C−H bond breaking step in the selective oxidation of propylene to acrolein is generally agreed upon as the rds in the literature,[14–17] there is not complete agreement with regard to which α-C−H bond breaking step is responsible for the rds: C−H bond breaking of propylene during chemisorption or the surface allyl intermediate during surface reaction. Researchers working with bulk bismuth molybdate catalysts have proposed that the methyl C−H bond breaking during propylene chemisorption is the rds.[6,45–47] Many of the studies with bulk bismuth molybdate catalysts also reported detecting surface allyl intermediates,[31,48–50] which is not consistent with the rds step involving propylene chemisorption since all steps subsequent to the rds should be very rapid.[51] In other words, there should not be any accumulation of surface allyl intermediates on the catalyst surface after the rds step of dissociative chemisorption of propylene. Accumulation of surface allyl intermediates on the catalyst surface should only occur if the formation of surface allyl precedes the rds. Furthermore, the constant surface C_3H_5*/C_3D_5* IR ratio in the 70−150 °C range reveals that breaking of the first α-C−H bond is not involved in the rds for propylene oxidation to acrolein over the supported V_2O_5/Nb_2O_5 catalyst.

Insights into the sequence of the oxygen insertion step relative to the second C−H bond breaking step are provided from comparative $H_2C{=}CHCH_3$-TPSR and $H_2C{=}CHCH_2OH$-TPSR experiments. Allyl alcohol chemisorbs via breaking the O−H bond to form the surface allyloxy ($H_2C{=}CHCH_2O$*) intermediate that decomposes to acrolein at 163 °C by breaking one of the two α-C−H bonds (see Figure 11). This reaction temperature for acrolein formation is significantly lower than for acrolein formation from propylene (~200 °C) and reveals that (*i*) kinetics for breaking of the C−H bond is accelerated by the presence of C−O bond and (*ii*) acrolein formation from C_3H_6 does not proceed *via* the surface allyloxy ($H_2C{=}CHCH_2O$*) intermediate. This is further substantiated by the corresponding *operando* IR spectra during propylene oxidation (see Figure 2) demonstrating that the surface C_3H_5* intermediate, and not the surface allyloxy ($H_2C{=}CHCH_2O$*) intermediate (see Figure 12), is present during propylene oxidation. Thus, lattice oxygen insertion into the surface C_3 hydrocarbon intermediate must take place after the second α-C−H bond breaking step to form surface $H_2C{=}CHCH$* or occurs in a concerted reaction with the second α-C−H bond breaking step.

From the above fundamental molecular level insights the following new reaction mechanism is proposed for the selective oxidation of propylene to acrolein over the well-defined model supported V_2O_5/Nb_2O_5 catalyst:

$$O_2 + 2* \leftrightarrow 2O* \quad K_{ads,O2} \tag{1}$$

$$CH_2{=}CH{-}CH_3 + O* + * \leftrightarrow CH_2{=}CH{-}CH_2* + HO* \quad K_{ads,C3H6} \tag{2}$$

$$CH_2{=}CH{-}CH_2* + O* \rightarrow CH_2{=}CH{-}CH* + OH* \quad k_{3,rds} \tag{3}$$

$$CH_2{=}CH{-}CH* + O* \rightarrow CH_2{=}CH{-}CH{=}O + 2* \quad k_4 \tag{4}$$

$$HO* + HO* \leftrightarrow H_2O + O* + * \quad K_{ads,H2O} \tag{5}$$

The first step is the reversible dissociative chemisorption of gas phase molecular O_2 on the catalyst surface to form reactive surface O* species. In the second step, propylene is reversibly dissociated and chemisorbed as surface CH_2CHCH_2* and HO* intermediates (L-H mechanism). The presence of surface O* is required to convert the surface H* to HO* and to prevent hydrogenation of the surface allylic intermediate back to propylene. The rds (step 3) involves C−H bond breaking of the surface allyl intermediate, which may be a concerted reaction step that occurs simultaneously with O* insertion (step 4). The surface O* for insertion, however, is supplied by the catalyst lattice oxygen (M-V-K mechanism). No attempt in the kinetics model is made for discriminating between the O* being supplied by the gaseous O_2 and the catalyst lattice O^{2-} species. The surface hydroxyl species formed during the two C−H bond breaking steps rapidly recombine to form H_2O (step 5). Subsequently, the reduced catalyst lattice sites become reoxidized, directly or indirectly, by the gaseous molecular O_2 to complete the catalytic cycle.

From the above elementary reaction steps and knowledge of the rds, the resulting reaction kinetics expression is obtained by applying the steady-state approximation:[51]

$$r = k_3 K_1^{1/2} K_2 [C_3H_6][O_2]^{1/2} \times \frac{[*]_0^2}{\left\{1 + 2K_1^{1/2}[O_2]^{1/2} + \frac{k_2[C_3H_6]}{k_{-2}+k_3} + \frac{k_2 k_3 [C_3H_6]}{k_4(k_{-2}+k_3)}\right\}^2} \tag{6}$$

in which $[*]_0$ represents the number of catalytic active sites (no. of sites/nm^2). This expression can be further simplified since $k_{-2} \gg k_3$ because k_3 is the rds, and K_1 and K_2 possess small values because the surface intermediate concentrations under elevated reaction conditions are minor (confirmed by *operando* IR spectroscopy measurements in Figure 2). Thus,

$$r = k_{rds} K_{ads} [C_3H_6][O_2^{1/2}][*]_0^2 \tag{7}$$

$$\text{and } K_{ads} = K_{ads,C3}(K_{ads,O2})^{1/2} \tag{8}$$

in which k_{rds} represents the kinetic rate constant for C−H bond breaking of the surface allyl C_3H_5* intermediate. The above

kinetic derivation also assumes that at steady-state the surface [*OH] concentration is comparable to the surface [O*] concentration under reaction conditions, which was required to match the observed kinetics. This kinetic expression is consistent with the experimentally observed reaction kinetics.[30] Interestingly, the same simplified kinetic expression is also obtained if it is assumed that the rds is the dissociative chemisorption of propylene, which shows that just kinetics can not be relied upon to discriminate between competing reaction mechanisms.[51] As already discussed above, the breaking of the second α-C−H bond of the surface allyl intermediate is the rds.

5. Conclusions

The combined *operando* Raman/IR/MS spectroscopy experiments, with the aid of isotopically labeled molecules ($^{18}O_2$ and C_3D_6), during propylene oxidation over the well-defined model supported V_2O_5/Nb_2O_5 catalyst affords a complete molecular level mechanistic determination of the selective oxidation of propylene to acrolein. The new insights reveal that propylene selective oxidation to acrolein proceeds via a combined Langmuir−Hinshelwood−Mars−van Krevelen surface reaction mechanism. The dissociative chemisorption of propylene forms surface CH_2CHCH_2* and HO* species and gas phase molecular O_2 is required to provide surface O* that oxidize the surface H* to HO* to prevent hydrogenation of the surface allyl intermediate back to propylene (L-H step). The insertion of O* into the surface allyl intermediate does not precede breaking of the second C−H bond and takes place either after or during this bond breaking step. The O* employed for oxygen insertion to form acrolein is exclusively supplied by catalyst lattice oxygen (M-V-K step). The rds involves breaking of the second surface allyl C−H bond and is responsible for the observed KIE of ∼3 for acrolein formation. The derived kinetics expression for propylene oxidation is in agreement with the experimentally observed kinetics for low concentrations of surface allyl species under reaction conditions at elevated temperatures.[30]

Acknowledgment. Financial support of this research by the U.S. Department of Energy-Basic Energy Sciences (Grant No. DE-FG02-93ER14350) is gratefully acknowledged. C.Z. gratefully acknowledges Dr. W. Lin and E. Lee for their advices on the execution of the *operando* spectroscopy experiments.

Appendix

Derivation of kinetics for the selective oxidation of propylene to acrolein over the supported V_2O_5/Nb_2O_5 catalyst.

$$O_2 + 2* \leftrightarrow 2\,O* \quad K_{ads,O2} \tag{1a}$$

$$CH_2{=}CH{-}CH_3 + O* + * \leftrightarrow CH_2{=}CH{-}CH_2* + HO* \quad K_{ads,C3H6} \tag{2a}$$

$$CH_2{=}CH{-}CH_2* + O* \rightarrow CH_2{=}CH{-}CH* + OH* \quad k_{3,rds} \tag{3a}$$

$$CH_2{=}CH{-}CH* + O* \rightarrow CH_2{=}CH{-}CH{=}O + 2* \quad k_4 \tag{4a}$$

$$HO* + HO* \leftrightarrow H_2O + O* + * \quad K_{ads,H2O} \tag{5a}$$

$$K_1 = \frac{[O*]^2}{[O_2][*]^2} \tag{1b}$$

$$\frac{d[C_3H_5*]}{dt} = k_2[C_3H_6][O*][*] - k_{-2}[C_3H_5*][HO*] - k_3[C_3H_5*][O*] = 0 \tag{2b}$$

$$\frac{d[C_3H_4*]}{dt} = k_3[C_3H_5*][O*] - k_4[C_3H_4*][O*] = 0 \tag{3b}$$

$$\text{from (1b)}: [O*] = K_1^{1/2}[O_2]^{1/2}[*] \tag{4b}$$

$$\text{from(2b)}: \quad [C_3H_5*] = \frac{k_2[C_3H_6][O*][*]}{k_{-2}[OH*] + k_3[O*]} \tag{5b}$$

$$\text{from(3b)}: \quad [C_3H_4*] = \frac{k_3[C_3H_5*]}{k_4} \tag{6b}$$

$$\text{From product acrolein}: \quad r = k_4[C_3H_4*][O*] \tag{7b}$$

Insert (6b) and (5b) into (7b): $r = k_4\frac{k_3[C_3H_5*]}{k_4}[O*] =$

$$k_3[C_3H_5*][O*] = k_3\frac{k_2[C_3H_6][O*][*]}{k_{-2}[OH*] + k_3[O*]}[O*]$$

Assume[OH*] = [O*], $r = k_3\frac{k_2[C_3H_6][O*][*]}{k_{-2}[O*] + k_3[O*]}[O*] =$

$$k_3\frac{k_2[C_3H_6][O*][*]}{k_{-2}+k_3} = k_3\frac{K_2[C_3H_6][O*][*]}{1 + k_3/k_{-2}} \tag{8b}$$

Insert (4b) into (8b): $r = k_3\frac{K_2[C_3H_6]K_1^{1/2}[O_2]^{1/2}[*]^2}{1 + k_3/k_{-2}}$ (9b)

Since $k_3 << k_{-2}$, $1 >> k_3/k_{-2}$. To simplify (9b):

$$r = k_3K_1^{1/2}K_2[C_3H_6][O_2]^{1/2}[*]^2 \tag{10b}$$

$$[*]_0 = [*] + [O*] + [C_3H_5*] + [OH*] + [C_3H_4*] \tag{11b}$$

Insert (4b−6b) and (8b) into (11b),

$$[*]_0 = [*] + 2K_1^{1/2}[O_2]^{1/2}[*] + \frac{k_2[C_3H_6][*]}{k_{-2}+k_3} + \frac{k_2k_3[C_3H_6][*]}{k_4(k_{-2}+k_3)} \tag{12b}$$

$$[*] = \frac{[*]_0}{1 + 2K_1^{1/2}[O_2]^{1/2} + \frac{k_2[C_3H_6]}{k_{-2}+k_3} + \frac{k_2k_3[C_3H_6]}{k_4(k_{-2}+k_3)}} \tag{13b}$$

Insert (13b) into (10b)

$$r = k_3k_1^{1/2}k_2[C_3H_6] \times [O_2]^{1/2}\frac{[*]_0^2}{\left\{1 + 2k_1^{1/2}[O_2]^{1/2} + \frac{k_2[C_3H_6]}{k_{-2}+k_3} + \frac{k_2k_3[C_3H_6]}{k_4(k_{-2}+k_3)}\right\}^2}$$

When $1 >> 2k_1^{1/2}[O2]^{1/2} + \frac{k_2[C_3H_6]}{k_{-2}+k_3} + \frac{k_2k_3[C_3H_6]}{k_4(k_{-2}+k_3)}$,

$$r = k_3k_1^{1/2}k_2[C_3H_6][O_2]^{1/2}[*]_0^2 \tag{14b}$$

References and Notes

(1) Dadyburjor, D. B.; Jewur, S. S.; Ruckenstein, E. *Catal. Rev.* **1979**, *19*, 293–350.
(2) Sachtler, W. M. H. *Rec. Trav. Chim. Pays-Bas* **1963**, *82*, 243.
(3) Keulks, G. W. *J. Catal.* **1970**, *19*, 232.
(4) Sancier, K. M.; Wentrcek, P. R.; Wise, H *J. Catal.* **1975**, *39*, 141–147.
(5) Miura, H.; Otsubo, T.; Shirasaki, T.; Morikawa, Y *J. Catal.* **1979**, *56*, 84.
(6) Moro-oka, Y.; Ueda, W *Adv. Catal.* **1995**, *40*, 233.
(7) Lieto, J. M.; Bielsa, R.; Kremenic, G.; Fierro, J.; Stud, L *Surf. Sci. Catal.* **1990**, *55*, 295.

(8) Al'kaeva, E. M.; Andrushkevich, T. V.; Yu Ovsitser, O.; Sokolovskii, V. D *Catal. Today* **1995**, *24*, 357.
(9) Grasselli, K. M. *J. Chem. Educ.* **1986**, *63*, 216.
(10) Burrington, J. D.; Grasselli, R. K *J. Catal.* **1980**, *63*, 235.
(11) Adams, C. R.; Jennings, T. J *J. Catal.* **1962**, *2*, 63.
(12) Adams, C. R.; Jennings, T. J *J. Catal.* **1964**, *3*, 549.
(13) Monnier, J. R.; Keulks, G. W *J. Catal.* **1981**, *68*, 51.
(14) Grasselli, R. K.; Burrington, J. D *Adv. Catal.* **1981**, *30*, 133.
(15) Arora, N.; Deo, G.; Wachs, I. E *J. Catal.* **1996**, *159*, 1.
(16) Kobayashi, M.; Futaya, R *J. Catal.* **1979**, *56*, 73.
(17) Martir, W.; Lunsford, J *J. Am. Chem. Soci.* **1981**, *103*, 3728.
(18) Schultz, J.; Beauchamp, J *J. Phys. Chem.* **1983**, *87*, 3587.
(19) Carrazan, S. R. G.; Martin, C.; Rives, V.; Vidal, R *Spec. Act. Part A: Mol. Bio. Spec.* **1996**, *52*, 1107.
(20) Grzybowska, B.; Haber, J.; Janas, J *J. Catal.* **1977**, *49*, 150.
(21) Orlov, A. N; Gagarin, S. G *Kinetika i Kataliz* **1974**, *15*, 1481.
(22) Mars, P.; van Krevelen, D. W. *Chem. Eng. Sci.* **1954**, *3*, 41.
(23) Thomas J. M., and Thomas W. J. *Principles and Practice of heterogeneous catalysis*; VCH Verlagsgesellschaft mbH: Weinheim, 1997.
(24) Voge, H. H. *Adv. Chem. Ser.* **1968**, *76*, 242.
(25) Feng, Y.; Gao, X.; Zhang, S.; Zhu, Y *Dalian Qinggongye Xueyuan Xuebao* **1999**, *18*, 141.
(26) Oyama, S. T.; Desikan, A. N.; Zhang, W *ACS Symposium Series* **1993**, *523* (Catalytic Selective Oxidation), 16–30.
(27) Fierro, J. L. G.; Gambaro, L. A.; Cooper, T. A.; Kremenic, G *Appl. Catal.* **1983**, *6*, 363.
(28) Li, M.; Shen J, *React. Kin. Catal. Lett.* **2001**, *72*, 263–267.
(29) Li, M.; Shen, J *J. Catal.* **2002**, *205*, 248–258.
(30) Zhao, C.; Wachs, I. E *Catal. Today* **2006**, *118*, 332.
(31) Song, Z.; Mimura, N.; Bravo-Suarez, J.; Akita, T.; Tsubota, S.; Oyama, S. T *Appl. Catal. A: General* **2007**, *316*, 142.
(32) Banares, M. A. *Catal. Today* **2005**, *100*, 71.
(33) Weckhuysen, B. M. *Chem. Phys. Phys. Chem.* **2003**, *5*, 4351.
(34) Davis, J. L.; Barteau, M. A *Surf. Sci.* **1990**, *235*, 235–48.
(35) Sambasivan, S.; Fischer, D. A.; DeKoven, B. M.; Kuperman, A *Adv. Mater.* **2000**, *12*, 1809.
(36) Gao, F.; Wang, Y.; Tysoe, W. T *J. Phys. Chem. B* **2006**, *110*, 12555.
(37) Levinson, J.; Kretzschmar, I.; Sheehy, M.; Deiner, L.; Friend, C *Surf. Sci.* **2001**, *479*, 273.
(38) Pushkarev, V. V.; Kovalchuk, V. I.; D'Itri, J. L *J. Phys. Chem. B* **2004**, *108*, 5341.
(39) Weckhuysen, B. M.; Jehng, J.; Wachs, I. E *J.Phys. Chem. B* **2000**, *104*, 7382–7387.
(40) Bertie, J. E.; Zhang, S. L *J. Chem. Phys.* **1994**, *101*, 8364.
(41) Rana, F. R.; Mautone, A. J.; Dluhy, R. A. *Biochem.* **1993**, *32*, 3169–77.
(42) Silvi, B.; Perchard, J. P *Spectrochim. Acta* **1976**, *32*, 11.
(43) Saleem, S. S.; Aruldhas G, *Ind. J. Pure Appl. Phys.* **1981**, *19*, 1088–91.
(44) Sanchez Escribano, V.; Busca, G.; Lorenzelli, V *J. Phys. Chem.* **1990**, *94*, 8939–45.
(45) Sampson, R. J.; Shooter, D *Oxid. Combust. Rev.* **1965**, *1*, 223.
(46) Grasselli, R. K. *Top. Catal.* **2002**, *21*, 79.
(47) Doornkamp, C.; and Ponec V, *J. Mol. Catal. A* **2000**, *162*, 19.
(48) Blatter, F.; Sun, H.; Frei, H *Catal. Lett.* **1995**, *35*, 1–12.
(49) Sanchez Escribano, V.; Busca, G.; Lorenzelli, V *J. Phys. Chem.* **1990**, *94*, 8939.
(50) Davydov, A. A.; Mikhal'chenko, V. G.; Sokolovskii, V. D.; Boreskov, G. K *J. Catal.* **1978**, *55*, 299–313.
(51) Boudart M., and Mariadassou G., *Kinetics of Heterogeneous Catalytic Reactions (Physical Chemistry: Science & Engineering)*; Princeton University Press: Princeton, NJ, 1984.

JP801562G